

This is the accepted manuscript made available via CHORUS. The article has been published as:

## Characterization of a chiral phase in an achiral bent-core liquid crystal by polarization studies of resonant x-ray forbidden reflections

V. Ponsinet, P. Barois, LiDong Pan, Shun Wang, C. C. Huang, S. T. Wang, R. Pindak, U. Baumeister, and W. Weissflog

Phys. Rev. E **84**, 011706 — Published 15 July 2011

DOI: [10.1103/PhysRevE.84.011706](https://doi.org/10.1103/PhysRevE.84.011706)

# **Characterization of a chiral phase in an achiral bent-core liquid crystal by polarization studies of resonant x-ray forbidden reflections**

**V. Ponsinet<sup>1</sup>, P. Barois<sup>1</sup>, LiDong Pan<sup>2</sup>, Shun Wang<sup>2</sup>, C.C. Huang<sup>2</sup>, S.T. Wang<sup>3</sup>, R. Pindak<sup>3</sup>, U.  
Baumeister<sup>4</sup> and W. Weissflog<sup>4</sup>**

<sup>1</sup>Centre de Recherche Paul Pascal, Université Bordeaux 1, CNRS, Av. A. Schweitzer, 33600 Pessac,  
France

<sup>2</sup>School of Physics and Astronomy, University of Minnesota, Minneapolis, Minnesota 55455, USA

<sup>3</sup>Brookhaven National Laboratory, National Synchrotron Light Source, Upton, New York 11973, USA

<sup>4</sup>Martin-Luther-Universität Halle-Wittenberg, Institut für Chemie, 06120 Halle, Germany

Abstract: The chiral antiferroelectric structure of an achiral bent-core liquid crystal is characterized for the first time by resonant x-ray scattering at chlorine K-edge. The “forbidden” reflections resulting from the glide or screw symmetry elements are restored by the anisotropy of the tensor structure factor which we calculate for two possible structural models. A careful analysis of the polarization states of the restored “forbidden” reflections enables an unambiguous identification of a chiral structure (i.e. the so-called anticlinic, antiferroelectric smectic-C or Sm-C<sub>A</sub>P<sub>A</sub>) co-existing with the achiral synclinic antiferroelectric smectic-C or Sm-C<sub>S</sub>P<sub>A</sub>. The method proves to be quite powerful as it identifies the chiral structure within coexisting phases despite an imperfect orientation of the sample. The volume fraction of the chiral phase and the distribution of alignment are extracted from the data.

PACS number(s): 61.30.Eb, 61.05.c

Thermotropic liquid crystals (LCs) are complex fluids resulting from low-dimensional self-organization of organic molecules of specific architecture (mesogens) generally constituted of a rigid core (imposing the global shape) surrounded by or terminated by flexible chains. The most common shapes of mesogens are rods and disks. In recent years, LCs made of bent-core molecules have attracted a lot of attention for their rich and complex polymorphism, and for unexpected physical properties such as ferroelectricity or the presence of twisted structures in achiral materials [1-3]. Unlike rod-like or disk-like mesogens, the description of the orientation of a bent-core molecule requires two vector fields [3], namely the string  $\mathbf{n}$  and the arrow  $\mathbf{b}$  in the convenient picture of a bow. The phases resulting from the spatial organization of these two fields have been assigned names  $B_1$  to  $B_7$  as they were discovered [4]. Among them, the so-called  $B_2$  phase shows a lamellar structure formed by a regular stack of liquid layers of thickness  $d$  along a direction  $Z$ . Four microscopic models have been proposed [Fig. 1] which correspond to the four combinations of the Sm-C-like tilt of the string (synclinic or anticlinic) and of the polarization borne by the arrow (ferroelectric or antiferroelectric). The general notation  $\text{Sm-C}_S \text{ or } \text{A}P_F \text{ or } \text{A}$  summarizes these four states. The in-plane axes  $X$  (along the tilt direction) and  $Y$  (along the arrow) complete the reference frame. Link et al. [5] have pointed out that the individual layers of the proposed structures are chiral (i.e. different from their mirror image) although the molecules are achiral. Two of the proposed structures are also chiral (namely  $\text{Sm-C}_S P_F$  and  $\text{Sm-C}_A P_A$ ) whereas  $\text{Sm-C}_S P_A$  and  $\text{Sm-C}_A P_F$  are racemic stacks of layers of opposite handedness.

From a crystallographic point of view, the unit cell is one layer for the  $\text{Sm-C}_S P_F$  structure but two layers of opposite tilt and/or polarization for the other three. In reciprocal space, the basic wave vector component  $Q_Z$  of the latter is then  $Q_0/2$ , with  $Q_0 = 2\pi/d$ . The half-order Bragg reflections (in  $Q_0$  units) are forbidden by the classical extinction rules [i.e. glide plane  $(X,Z)$  for the  $\text{Sm-C}_S P_A$  phase, glide plane  $(Y,Z)$  for  $\text{Sm-C}_A P_F$ , and  $2_1$  screw axis for  $\text{Sm-C}_A P_A$ ] which implies that the four structures cannot be distinguished by conventional diffraction of x-rays.

It was shown in a previous work [6] that resonant x-ray diffraction (RXRD) could be used to overcome this problem. Indeed, the half-order forbidden reflections were observed (hence ruling out the  $\text{Sm-C}_S P_F$  phase) and a careful analysis of their polarization state enabled the unambiguous characterization of the  $\text{Sm-C}_S P_A$  phase.

However, electro-optical studies of various  $B_2$  phases found in other materials claimed that different structures may exist, depending on the electrical history of a sample [4]. Reports by Barnik *et al.* [7] on the possible coexistence of two antiferroelectric  $B_2$  phases in a bent-core material were particularly

intriguing. The coexistence of two phases over an extended temperature range in a pure compound is in principle forbidden by the phase rule. It may however occur in thin films if the interaction with the surfaces stabilizes a second phase or if metastable states are trapped by slow kinetics. The present work is devoted to a structural characterization by resonant scattering of the bent-core material studied in ref. [7]. The aim of our study is to characterize unambiguously the reported Sm-C<sub>A</sub>P<sub>A</sub> structure and determine whether it appears in a pure phase or in coexisting phases.

The bent-core liquid crystal studied is the homolog (n=14) of the series 4-chloro-1,3-phenylene bis[4-(4-n-alkylphenyl-iminomethyl) benzoate] [8] (or 14 PBCl for short). The molecular structure is given in Fig. 2. The two-layer super-structure of the B<sub>2</sub> phase of this material was first confirmed by resonant scattering [9]. The Sm-C-like tilt angle  $\alpha$  was measured independently by conventional x-ray scattering on oriented samples yielding an experimental value of  $28^\circ \pm 3^\circ$ . Electro-optical studies of this material [10] exhibited an anti-ferroelectric response but optical observations showed the presence of circular domains rotating in opposite directions under field, hence revealing the presence of chiral domains of opposite handedness. This observation, not consistent with the achiral Sm-C<sub>S</sub>P<sub>A</sub> structure, suggests a Sm-C<sub>A</sub>P<sub>A</sub> phase instead.

**THEORETICAL BACKGROUND.** The technique of resonant scattering was successfully applied to resolve the structure of chiral [11,12] and bent-core [6] liquid crystals. Let us recall briefly that resonant (or anomalous) x-ray scattering occurs when the energy of the x-ray radiation approaches the values required to excite an inner-shell electron into an empty state of the outer shell [13]. In such circumstances, the atomic scattering factor  $f_a$  exhibits a complex frequency-dependent contribution in addition to the classical (non resonant) term  $f_0$ , which is the Fourier transform of the electron density. The resonant contribution depends on the atom and becomes substantial near its absorption edges. Because of the local anisotropy of the outer shell unoccupied states, the resonant structure factor is a tensor that reflects the symmetry of the resonant atom within the molecule. The anisotropy of this tensor leads to the observation of forbidden reflections and determines their non trivial polarization properties. The variations of the polarization state and of the intensity of the resonant forbidden reflections have been worked out by V.E. Dmitrienko as a function of the rotation angle  $\phi$  of the sample about the scattering vector  $\mathbf{Q}$  for cubic crystals in kinematic theory [14]. This theoretical work was used in reference [6] to characterize the Sm-C<sub>S</sub>P<sub>A</sub> structure. Let us recall how it applies to the structures of the B<sub>2</sub> phases.

The structure factor tensor was derived in each phase from the basic symmetries of the molecule and of the unit cell. For the half order forbidden reflections of the two antiferroelectric phases, the tensors have the form [6]:

$$\tilde{\tilde{F}}(SmC_sP_A) = \begin{bmatrix} 0 & iA \sin \alpha & 0 \\ iA \sin \alpha & 0 & iA \cos \alpha \\ 0 & iA \cos \alpha & 0 \end{bmatrix} \quad (1a)$$

$$\tilde{\tilde{F}}(SmC_A P_A) = \begin{bmatrix} 0 & 0 & B \sin 2\alpha \\ 0 & 0 & iA \cos \alpha \\ B \sin 2\alpha & iA \cos \alpha & 0 \end{bmatrix} \quad (1b)$$

$A$  and  $B$  are unknown complex numbers and  $\alpha$  is the tilt angle of the string with respect of the axis  $Z$  (layer normal). The scattering amplitudes  $\bar{A}_{\gamma\delta}$  derive simply from the tensors via the usual formulae [14]:

$$\bar{A}_{\gamma\delta} = \gamma \cdot \tilde{\tilde{F}} \delta \quad (2)$$

in which the incident and diffracted polarization vectors  $\delta$  and  $\gamma$  can take the two values  $\pi$  (in the scattering plane) or  $\sigma$  (perpendicular to the scattering plane). The scattering geometry is shown in Fig. 2. In our experiment, the incident beam is  $\sigma$ -polarized so that the incident  $\pi$ -polarization is not considered.

The polarization state of the resonant Bragg peaks hence depends on the orientation  $\varphi$  of the sample [14]. The general form of the scattered intensity can be expressed as [6]:

$$I(\varphi, \chi) / A^2 \sin^2 \alpha = a_\sigma^2 \cos^2 \chi + a_\pi^2 \sin^2 \chi + 2a_\sigma a_\pi \sin \chi \cos \chi = (a_\sigma^2 + a_\pi^2) \cos^2(\chi - \omega) \quad (3)$$

with  $a_\sigma = -\bar{A}_{\sigma\sigma}/iA \sin \alpha$ ,  $a_\pi = -\bar{A}_{\sigma\pi}/iA \sin \alpha$  and  $\omega = \arctan(a_\pi/a_\sigma)$ .

In the  $Sm-C_sP_A$  phase, the rescaled coefficients are both real :  $a_\sigma = a_{S,\sigma} = \sin 2\varphi$  and  $a_\pi = a_{S,\pi} = (\sin \theta_B \cos 2\varphi - \cos \theta_B \cos \varphi / \tan \alpha)$

In the  $Sm-C_A P_A$  phase,  $a_{A,\sigma} = 0$  and  $a_{A,\pi} = -\cos \theta_B \cos \varphi / \tan \alpha - 2iB/A \cos \alpha \cos \theta_B \sin \varphi$ .

Here  $\theta_B$  is the Bragg angle of the resonant peak chosen at  $Q_z = 3/2 Q_0$  to avoid the strong reflected background at  $1/2 Q_0$ .

The polarization of the resonant peaks is hence linear and rotated by an angle  $\omega$  with respect to the polarization direction of the incident x-rays in the two antiferroelectric phases of interest namely Sm-C<sub>S</sub>P<sub>A</sub> and Sm-C<sub>A</sub>P<sub>A</sub>:

$$\omega(\varphi) = \arctan[(\sin \theta_B \cos 2\varphi - \cos \theta_B \cos \varphi / \tan \alpha) / \sin 2\varphi] \quad \text{for Sm-C}_S\text{P}_A \quad (4)$$

and  $\omega(\varphi) = \pi/2$  for Sm-C<sub>A</sub>P<sub>A</sub>

The expected variations  $\omega(\varphi)$  are plotted in Fig 3.

**EXPERIMENTS.** The experimental conditions are similar to those described in reference [6]. The bent-core LC material 14PBCl exhibits the following phase sequence on cooling: isotropic - 127°C - B<sub>2</sub> - 68°C - crystal [8]. It was spread in the B<sub>2</sub> phase by shearing a drop of the material along one direction on a 12 × 12 mm<sup>2</sup> glass substrate treated by deposition of a thin layer of surfactant (hexadecyl trimethyl ammonium bromide). The x-ray experiments were carried out at beam line X-19A of the National Synchrotron Light Source. A complete description of the three-circle diffraction set up was given in an earlier paper [12]. The LC sample was mounted on an additional motorized  $\phi$  rotation stage around the Z axis fitted inside a two-stage oven allowing 20 mK resolution in temperature. The polarization of the diffracted beam could be analyzed by a pyrolytic graphite crystal mounted on the two-theta arm. The beam size was set to 200 (vertical) × 500 (horizontal) μm<sup>2</sup>, and the  $\Delta Q_z$  resolution was  $1.9 \times 10^{-3} \text{ \AA}^{-1}$ . A fluorescence energy scan was first performed to tune the energy to the chlorine *K* edge at 2.823 keV.

The x-ray diffraction experiments were performed at  $T = 76.36^\circ\text{C}$  in the B<sub>2</sub> phase. The forbidden Bragg reflexion at  $Q_z = 3/2 Q_0$  was first recorded without the analyzer crystal. In this geometry, both components  $\sigma$  and  $\pi$  of the diffracted beams are collected. Figure 4 shows a typical scan of the intensity scattered along the direction  $Q_z$  perpendicular to the smectic layers. It shows a sharp resonant 3/2 reflexion superimposed on a background scattering that slowly decays with  $Q_z$ . This non resonant background is mainly due to the reflectivity of the air-liquid crystal interface and may contain contributions from the Kapton windows and helium gas in the flight path. The layer thickness  $d$  was 46.9 Å. Transverse theta scans across the Bragg peaks showed that the alignment of the layers was better than 0.02°.

The polarization of the Bragg peaks was then recorded by rotating the polarimeter about the direction  $\mathbf{k}_d$  of the diffracted beam. The rotation axis of the polarimeter was first carefully aligned along  $\mathbf{k}_d$  through a couple of 0.5 mm pinhole apertures. In order to avoid a possible mechanical bias, a rocking scan of the graphite crystal was performed for each value of the polarimeter angle  $\chi$ .

The linear  $\sigma$  polarization of the incident synchrotron beam and of the non resonant (001) and (002) Bragg peaks were checked first, defining the origin of the polarimeter angle  $\chi = 0$  on a maximum of intensity. The extinction was almost complete (residual intensity was about 1.5%-3.5% of the maximum intensity) and consistent with the less than optimal Bragg angle  $\theta_{BCrystal} = 40.5^\circ$  of the graphite crystal.

The polarization of the 3/2 resonant peak was then investigated for different values of  $\varphi$ . Figure 5 shows for example the intensity of the resonant signal vs. rotation  $\chi$  of the analyzer crystal for the same sample position as in Fig. 4,  $\varphi = 150^\circ$ .

For each value of  $\varphi$ , the experimental signal can be fitted to the following function:

$$I_{\text{exp}}(\varphi, \chi) = A2_m \cos^2 \chi + B2_m \sin^2 \chi + 2C_m \sin \chi \cos \chi \quad (5)$$

This expression cannot be simply identified with Eq. 3 since the experimental values of  $A2_m$ ,  $B2_m$  and  $C_m$  do not satisfy the condition  $C_m^2 = A2_m B2_m$  and the data must be corrected for background contributions.

First of all, the  $\sigma$ -polarized background appearing in  $Q_z$  scans (Fig 4) contributes a term  $Y(\varphi)\cos^2 \chi$  to the scattering. Adding this term to Eq. 3 and averaging over  $\chi$  yields the intensity recorded without analyzer crystal:

$$I^{Nocrystal}(\varphi) = (a_\sigma^2 + a_\pi^2)/2 + Y/2 \quad (6)$$

The background to signal ratio  $R$  extracted from the experimental  $Q_z$  scan is then:

$$R = Y/(a_\sigma^2 + a_\pi^2) \quad (7)$$

A weaker correction arises from the less than optimal analyzer crystal angle which transmits a factor  $\cos^2(2\theta_{BCrystal}) = 0.024$  of the polarization orthogonal to its main axis. This contributes a term  $\cos^2(2\theta_{BCrystal}) (a_\sigma^2 \cos^2 \chi + a_\pi^2 \sin^2 \chi - 2a_\sigma a_\pi \sin \chi \cos \chi)$  to the scattering in Eq. 3.

Subtracting these two contributions from Eq.5 yields the new parameters  $A2$ ,  $B2$ ,  $C$  corrected for background scattering and analyzer crystal Bragg angle:

$$\begin{aligned} A2 &= \frac{A2_m (1 + R \cos^2(2\theta_{BCryst})) - B2_m (\cos^2(2\theta_{BCryst}) + R)}{(1 + R) \sin^2(2\theta_{BCryst})} \\ B2 &= \frac{B2_m - A2_m \cos^2(2\theta_{BCryst})}{\sin^2(2\theta_{BCryst})} \quad C = \frac{C_m}{\sin^2(2\theta_{BCryst})} \end{aligned} \quad (8)$$

Finally, the imperfection of the in-plane alignment of the sample must be accounted for. The most general case can be described by a distribution function  $\mathcal{P}(\varphi')$  that measures the density of probability of a local in-plane orientation of the tilt at an angle  $\varphi'$  away from the direction of shear. The unknown function  $\mathcal{P}$  is expected to be even and have a maximum at  $\varphi'=0$  by symmetry. Convoluting this function with Eq.3 yields the intensity scattered by an imperfectly aligned phase:

$$\langle I(\varphi, \chi) \rangle = A2 \cos^2 \chi + B2 \sin^2 \chi + 2C \sin \chi \cos \chi \quad (9)$$

with

$$\begin{aligned} A2(\varphi) &= \int_{-\pi}^{\pi} d\varphi' \mathcal{P}(\varphi') a_\sigma^2(\varphi - \varphi'), \quad B2(\varphi) = \int_{-\pi}^{\pi} d\varphi' \mathcal{P}(\varphi') a_\pi^2(\varphi - \varphi') \\ \text{and} \quad C(\varphi) &= \int_{-\pi}^{\pi} d\varphi' \mathcal{P}(\varphi') a_\sigma(\varphi - \varphi') a_\pi(\varphi - \varphi') \end{aligned} \quad (10)$$

Equations 8-10 hence yield the wanted relationship between the measured parameters  $A_m$ ,  $B_m$ ,  $C_m$  and the theoretical formulae (Eq.3). The experimental orientation  $\omega_{exp}$  of the polarization corresponds to the maxima of Eq.9. Simple trigonometric algebra yields:

$$\tan \omega_{exp} = \text{sign}(C) |b/a| \quad (11)$$



with  $a^2 = (A2 - B2 + \sqrt{(A2 - B2)^2 + 4C^2})/2$  and  $b^2 = (B2 - A2 + \sqrt{(A2 - B2)^2 + 4C^2})/2$

The rotation  $\omega_{exp}$  of the polarization is plotted in Fig. 6 vs.  $\varphi$ . The strong variation of  $\omega_{exp}$  with  $\varphi$  clearly rules out the pure Sm-C<sub>A</sub>P<sub>A</sub> model (i.e.  $\omega_{exp} = 90^\circ$  for all  $\varphi$ ). Moreover, we found that the experimental data could not be fitted to the Sm-C<sub>S</sub>P<sub>A</sub> model with any possible width and shape of the distribution function  $\mathcal{P}(\varphi')$ . As an illustration, the dotted line in Fig. 6 is calculated from Eqs. 9-10 with a Gaussian function  $\mathcal{P}(\varphi')$  of width  $15^\circ$  (FWHM).

We then tried to fit our data to a model of coexisting Sm-C<sub>S</sub>P<sub>A</sub> and Sm-C<sub>A</sub>P<sub>A</sub> phases. In such case, the theoretical intensity of resonant scattering follows from Eq.3:

$$I_{mix}(\varphi, \chi) = (1 - f_{Vol})a_{S,\sigma}^2 \cos^2 \chi + \left[ (1 - f_{Vol})a_{S,\pi}^2 + f_{Vol}|a_{A,\pi}|^2 \right] \sin^2 \chi + 2(1 - f_{Vol})a_{S,\sigma}a_{S,\pi} \sin \chi \cos \chi \quad (12)$$

in which  $f_{Vol}$  is the volume fraction of the Sm-C<sub>A</sub>P<sub>A</sub> phase in the mixture. We assume that the typical size of the Sm-C<sub>S</sub>P<sub>A</sub> and Sm-C<sub>A</sub>P<sub>A</sub> regions is larger than the coherence length  $\xi \sim 300$  nm of the x-ray beam, so that intensities rather than amplitudes are added.

The  $\pi$ -polarized contribution of the Sm-C<sub>A</sub>P<sub>A</sub> phase can be rewritten as:

$$f_{Vol}/(1 - f_{Vol})|a_{A,\pi}|^2 = p \sin^2 \varphi + q \cos^2 \varphi + 2r \sin \varphi \cos \varphi \quad (13)$$

with

$$p = f_{Vol}/(1 - f_{Vol}) \eta^2 \cos^2 \alpha \cos^2 \theta_B \quad (14a)$$

$$q = f_{Vol}/(1 - f_{Vol}) \cos^2 \theta_B / \tan^2 \alpha \quad (14b)$$

$$r = f_{Vol}/(1 - f_{Vol}) \eta \cos \psi \cos^2 \theta_B \cos^2 \alpha / \sin \alpha \quad (14c)$$

in which  $\eta$  and  $\psi$  are the modulus and phase of the unknown complex factor  $2iB/A = \eta \exp(i\psi)$ .

Figure 6 shows a fit of the experimental data to this model. The dashed line is calculated for a perfectly oriented sample. The solid line is the best fit obtained with a Gaussian distribution of the in-plane orientation of width  $15 \pm 1^\circ$  (FWHM),  $p = 0.118 \pm 0.002$ ,  $q = 1.80 \pm 0.01$  and  $r = 0.026 \pm 0.002$ .

Figure 6 clearly shows that the model of coexisting Sm-C<sub>S</sub>P<sub>A</sub> and Sm-C<sub>A</sub>P<sub>A</sub> phases is fully consistent with the experimental data. We checked that the quality of the fit is not sensitive to the exact profile of the distribution function (i.e. Gaussian or simple gate function gives similar results).

The volume fraction of the Sm-C<sub>A</sub>P<sub>A</sub> phase can be estimated from Eq.14b which yields  $f_{\text{Vol}} = 34 \pm 6\%$ . The large uncertainty is mostly due to the error bar on the value of the tilt angle  $\alpha = 28 \pm 3$  degrees.

In conclusion, the present work provides the first direct evidence of the existence of the chiral Sm-C<sub>A</sub>P<sub>A</sub> structure in the B<sub>2</sub> phase of the 14PBCl material. We confirm that it coexists with the non chiral Sm-C<sub>S</sub>P<sub>A</sub> phase, in agreement with electro-optical studies of Barnik *et al.* [7]. The observation of the coexistence in two different geometries (closed cell in [7] and free surface in the present study) confirms that the two phases have very similar free energies: it is actually impossible to tell which of them corresponds to the ground state.

Research at the NSLS, BNL, was supported in part by the U.S. Department of Energy, Division of Materials Sciences and Division of Chemical Sciences, under contract No. DE-AC02-98Ch-0886. The research was supported in part by the National Science Foundation, Solid State Program, under Grant No. DMR-0605760. VP acknowledges financial support from CNano-GSO for experiments at NSLS.

---

### References:

- [1] T.Niori, T Sekine, J. Watanabe, T. Furukawa, and H. Takezoe, J. Mater. Chem. **6**, 1231 (1996).
- [2] G.Pelzl, S. Diele, and W. Weissflog, Adv. Mater. **11**, 707 (1999).
- [3] H.R. Brand, P.E. Cladis, and H. Pleiner, Eur. Phys. J. B. **6**, 347 (1998).
- [4] R.A. Reddy and C. Tschierske, J. Mater. Chem. **16**, 907 (2006).
- [5] D.R. Link, G. Natale, R. Shao, J.E. MacLennan, N.A. Clark, E. Korblova, D.M. Walba DM, Science **278**, 1924 (1997).
- [6] P. Fernandes, P. Barois, S. T.Wang, Z. Q. Liu, B. K. McCoy, C. C. Huang, R. Pindak, W. Caliebe, and H. T. Nguyen, Phys. Rev. Lett. **99**, 227801 (2007).
- [7] M.I. Barnik, L.M. Blinov, N.M. Shtykov, S.P. Palto, G. Pelzl and W. Weissflog, Liq. Cryst., **29**, 597 (2002).
- [8] W. Weissflog, C. Lischka, S. Diele, G. Pelzl and I. Wirth, Mol. Cryst. Liq. Cryst. **328**, 101 (1999).

- [9] A. Cady, R. Pindak, W. Caliebe, P. Barois, W. Weissflog, H.T. Nguyen and C.C. Huang, *Liq. Cryst.* **29**, 1101 (2002).
- [10] L.M. Blinov, M.I. Barnik, E.S. Bustamante, G. Pelzl, and W. Weissflog, *Phys. Rev. E* **67**, 021706 (2003).
- [11] P. Mach, R. Pindak, A.M. Levelut, P. Barois, H.T. Nguyen, C.C. Huang, L. Furenlid, *Phys. Rev. Lett.* **81**, 1015 (1998).
- [12] P.Mach, R. Pindak, A.M. Levelut, P. Barois, H.T. Nguyen, H. Baltes, M. Hird, K. Toyne, A. Seed, J.W. Goodby, C.C. Huang, L. Furenlid, *Phys. Rev. E* **60**, 6793 (1999).
- [13] J. L. Hodeau, V. Favre-Nicolin, S. Bos, H. Renevier, E. Lorenzo, J.F. Berar, *Chem. Rev.* **101**, 1843 (2001).
- [14] V. E. Dmitrienko, *Acta Crystallogr. Sect. A* **39**, 29 (1983).

### Figure captions:

FIG.1. (Color online). Sketch of the four possible structures of the  $B_2$  phase. The arrows show the polarization within each layer. The unit cell is two layers for structures 2, 3 and 4.

FIG.2. (Color online). Top: experimental scattering geometry. The  $\pi$ -component of the polarization of the incident x-ray beam is null. The polarization of the diffracted beam is analyzed by a pyrolytic (002) graphite crystal. The black arrow on sample denotes the direction of shear of the liquid crystal film. Bottom: chemical formula of the 14PBCl liquid crystal.

FIG.3. (Color online). Rotation  $\omega$  of the polarization vs. rotation  $\phi$  of the sample calculated for the two antiferroelectric  $B_2$  phases. The  $\text{Sm-C}_5\text{P}_A$  curve is calculated with Eq.4 for the true experimental values of the Bragg angle of the 3/2 resonant reflection  $\theta_B = 4.07$  deg and of the tilt angle  $\alpha = 28^\circ$  with no adjustable parameter.

FIG.4. (Color online). Normalized  $Q_z$  scan across the 3/2 resonant peak without polarizer crystal at chlorine K-edge. The dashed line is a fit to a Gaussian profile superimposed on a slowly decaying background. Inset shows a wider scan displaying the non resonant (001) ( $\times 10^{-5}$ ) and (002) ( $\times 1/25$ ) Bragg peaks.

FIG.5. (Color online). Polarimeter scan  $I(\phi=150^\circ, \chi)$  recorded on the resonant peak shown in Fig. 3. The data points (open circles) are fitted to Eq. 5 (dashed line). The solid line shows the corrected function after subtraction of the  $\sigma$ -polarized background and less than optimal analyzer angle correction (Eq. 9). The residual value of the minima is due to the imperfect in-plane orientation of the sample.

FIG.6. (Color online). Experimental rotation of the polarization of the 3/2 resonant Bragg peak  $\omega_{exp}$  vs. sample rotation  $\phi$ . Different symbols correspond to different samples of the same material. The dashed and solid lines are the best fits to the model of coexisting  $\text{Sm-C}_5\text{P}_A$  and  $\text{Sm-C}_A\text{P}_A$  phases with perfect in-plane alignment (dashed) and with a Gaussian distribution of in-plane orientation of width  $15 \pm 1^\circ$  (solid) for  $p = 0.118 \pm 0.002$ ,  $q = 1.80 \pm 0.01$  and  $r = 0.026 \pm 0.002$ . The dotted line is the polarization calculated for the pure  $\text{Sm-C}_5\text{P}_A$  phase with the same distribution of in-plane orientation and no other free parameter.

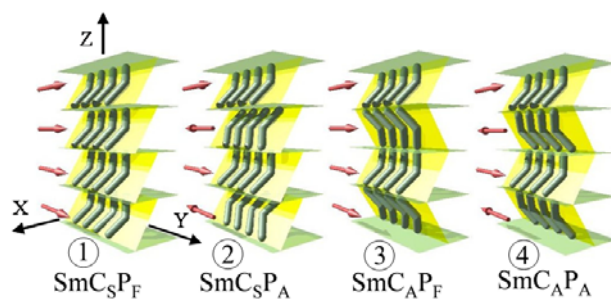


Figure 1

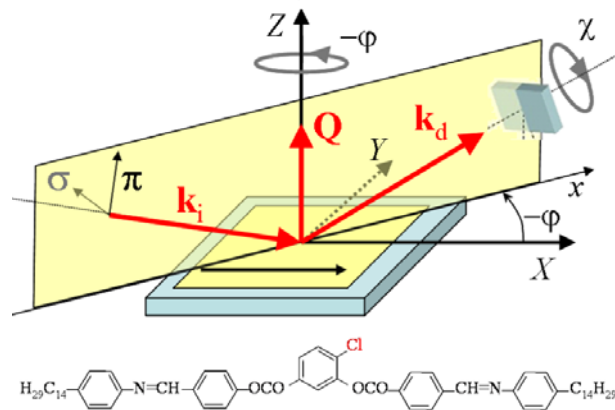


Figure 2

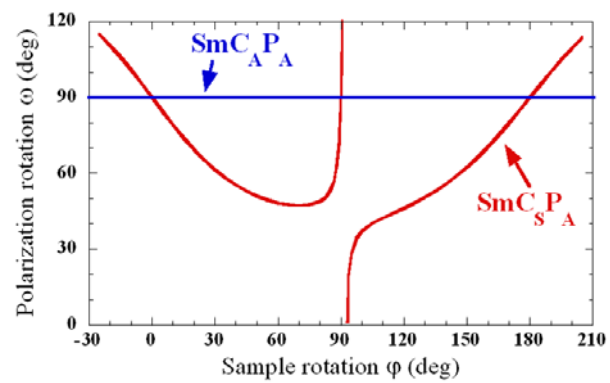


Figure 3

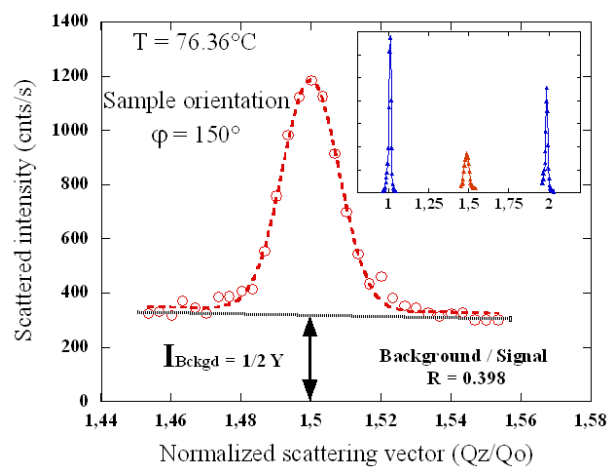


Figure 4

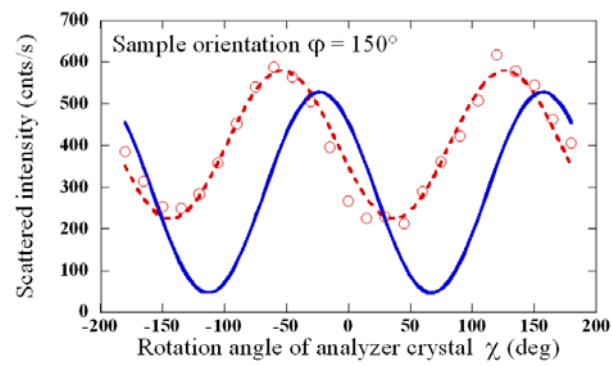


Figure 5

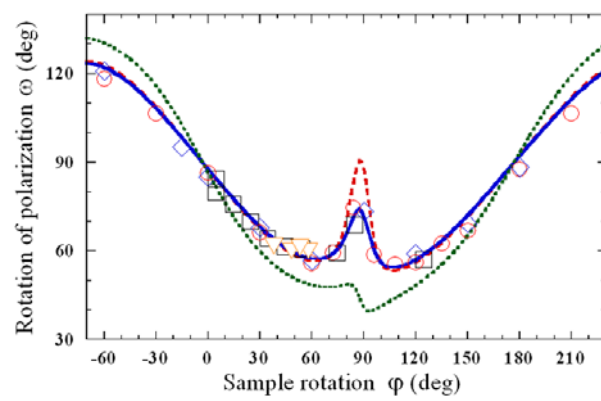


Figure 6